

Article

Detailed Landslide Traces Database of Hancheng County, China, Based on High-Resolution Satellite Images Available on the Google Earth Platform

Junlei Zhao ^{1,2}, Chong Xu ^{1,3,*}  and Xinwu Huang ²

¹ National Institute of Natural Hazards, Ministry of Emergency Management of China, Beijing 100085, China; 13126610323@163.com

² School of Engineering and Technology, China University of Geosciences (Beijing), Beijing 100083, China; huangxw@cugb.edu.cn

³ Key Laboratory of Compound and Chained Natural Hazards Dynamics, Ministry of Emergency Management of China, Beijing 100085, China

* Correspondence: xc1111111@126.com

Abstract: Hancheng is located in the eastern part of China's Shaanxi Province, near the west bank of the Yellow River. It is located at the junction of the active geological structure area. The rock layer is relatively fragmented, and landslide disasters are frequent. The occurrence of landslide disasters often causes a large number of casualties along with economic losses in the local area, seriously restricting local economic development. Although risk assessment and deformation mechanism analysis for single landslides have been performed for landslide disasters in the Hancheng area, this area lacks a landslide traces database. A complete landslide database comprises the basic data required for the study of landslide disasters and is an important requirement for subsequent landslide-related research. Therefore, this study used multi-temporal high-resolution optical images and human-computer interaction visual interpretation methods of the Google Earth platform to construct a landslide traces database in Hancheng County. The results showed that at least 6785 landslides had occurred in the study area. The total area of the landslides was about 95.38 km², accounting for 5.88% of the study area. The average landslide area was 1406.04 m², the largest landslide area was 377,841 m², and the smallest landslide area was 202.96 m². The results of this study provides an important basis for understanding the spatial distribution of landslides in Hancheng County, the evaluation of landslide susceptibility, and local disaster prevention and mitigation work.

Keywords: Hancheng County; human-machine interactive visual interpretation; landslides database; Google Earth platform



Citation: Zhao, J.; Xu, C.; Huang, X. Detailed Landslide Traces Database of Hancheng County, China, Based on High-Resolution Satellite Images Available on the Google Earth Platform. *Data* **2024**, *9*, 63. <https://doi.org/10.3390/data9050063>

Academic Editor: Juanle Wang

Received: 29 February 2024

Revised: 25 April 2024

Accepted: 27 April 2024

Published: 29 April 2024



Copyright: © 2024 by the authors. Licensee MDPI, Basel, Switzerland. This article is an open access article distributed under the terms and conditions of the Creative Commons Attribution (CC BY) license (<https://creativecommons.org/licenses/by/4.0/>).

1. Introduction

The term landslide usually refers to a geological structure displacement change phenomenon in which a soil block on a slope moves downward along the fragile zone of the slope under the action of its gravity due to the influence of factors such as rainfall erosion, ground vibration, and human engineering activities. Landslides often cause serious economic losses and casualties [1–3]. China has one of the worst landslide records of any country in the world. Since the 1980s, given the rapid development of the social economy, the increase in human engineering activities, and the influence of natural factors, landslide disasters have been increasing year by year [4–6]. Therefore, research on landslides can provide an important scientific guarantee for future disaster prevention and control. In landslide research, the establishment of a landslide database is a fundamental and basic element [7,8]. A complete landslide database is of great significance for the study of landslide distribution law, susceptibility assessment, and follow-up risk assessment [9,10].

So far, scholars from all over the world have conducted extensive research on landslide disasters. For example, Harp et al. established strict requirements for cataloguing and

interpreting landslides [11]. Pennington et al. established a national landslide database in the United Kingdom [12], which Taylor et al. improved [13]. Yasin Wahid Rabby et al. created a dataset of landslides in the Chittagong Hills of Bangladesh from January 2001 to March 2017, containing 730 landslides [14]. This was the first list of landslides covering the entire area of the Chittagong Hills in Bangladesh, and is of great significance for understanding the characteristics of landslides in the Chittagong Hills in the future. Alina Bejenaru created a list of landslides in the Crasna catchment area on the Romanian Moldovan plateau. The basin covers an area of 185.2 km², and 1619 landslides have been identified [15]. This landslide inventory also contains morphologically inferred landslide-type data, revealing the topography and the control role of landslide development. Francesco Fusco et al. reconstructed a revised list of landslides in the Campania region, including 83,284 landslides, by processing several existing landslide inventories for the region [16]. This inventory provides a new geodatabase that overcomes the problem of the coexistence of multiple lists.

China's plateau has a high altitude and many mountains, and these terrains generally have complex geological conditions and harsh climatic environments, resulting in frequent landslide disasters. After a detailed field survey of the landslide caused by the 2013 Lushan earthquake, Xu Chong et al. compiled a detailed and complete landslide catalog by interpreting remote sensing images through manual visual interpretation [17]. Pan Junwei carried out artificial visual interpretation and identification of ancient landslides in the eastern section of the Jiangnan Orogenic Belt in China (spanning the Jiangxi, Anhui, and Zhejiang provinces in China) [18], and established a database of 5047 landslides with a total area of 527 km², of which the largest single landslide area reached 1,475,697 m². For the 2022 Luding 6.8 magnitude earthquake, Huang et al. defined the range of intensity above VII as the study area and interpreted a total of 5007 coseismic landslides with a total area of 17.36 km². This landslide list supported a series of subsequent research works [19]. Based on the data collected from 1300 landslide sites, Hong et al. established a landslide database management system in Gansu Province using a computer, and comprehensively analyzed the regional distribution and geological characteristics of landslides in Gansu Province based on the results of computer data processing [20]. Hancheng County in Shaanxi Province is located on the Loess Plateau in China, with complex and fragmented topography. Hancheng is an important coal development base in Shaanxi Province and has a long history of coal development, and the goaf generated during coal mining has caused many landslides [21]. Previous work in the Hancheng area has focused more on the analysis and management of the deformation mechanisms of individual landslides, but there has been no landslide survey of the entire area, and the area lacks a complete landslide database [22–24]. To fill this gap, this study used high-resolution remote sensing satellite images from Google Earth to visually interpret landslides in the area and establish a complete and current landslide traces database. The results of this study provide a data-supported basis for understanding the development characteristics of landslides in Hancheng County.

2. Study Area

As shown in Figure 1, Hancheng is located in the northeast of the Guanzhong Plain in Shaanxi Province, adjacent to Heyang in the southeast, Yichuan in the north, Huanglong in the west, and Shanxi Province on the east side, separated by the Yellow River in the east of the study area, with geographical coordinates of 110°07'19"~110°37'24" east longitude and 35°18'50"~35°52'08" north latitude. The total area of the study area is about 1621 km², and the overall topographic characteristics are high in the northwest and low in the southeast [25]. The topography mainly includes middle mountainous areas, low mountains and hilly areas, loess plateau areas, and river valley terrace areas. The study area contains the famous Longmen Mountain, which is located in the northeast, about 30 km away from the urban area. The highest peak reaches 892 m; the height trend is northeast to southwest, and the altitude of the other peaks is more than 600 m. Due to the unique topography of the area, coupled with the large scale and longevity of the underground excavation work in the

area, many geological disasters such as landslides have been triggered. It is worth noting that many rivers traverse the land, and among these rivers, the three with the widest basin area are the Lingshui River, the Pan River, and the Chikai River, which together have a length of about 137.3 km. Each river converges in the Yellow River, which flows through the Loess Plateau with loose soils, so Hancheng has serious soil erosion problems, providing favorable conditions for landslides. There are two main types of geological structures in Hancheng: faults and folds. The most important fault is the Hancheng fault, which is inclined to the southeast, and the strike is northerly to northeastward, with a total length of hundreds of kilometers. The Hancheng fault is marked in Figure 1. According to the results of landslide interpretation, landslides are more distributed in the area around the Hancheng fault. The widely distributed rock formations in the area are mainly composed of sandstones from the Quaternary of the Cenozoic. In terms of climate type, Hancheng belongs to a warm temperate semi-arid continental monsoon climate, with mild climate conditions and sufficient sunshine conditions. The average temperature is about 13 °C. There is more rainfall in this area, but the precipitation distribution is very uneven; the high rainfall period lasts 7–9 months, and the maximum rainfall is generally distributed around August. In addition, the rainfall shows a trend of decreasing from north to south in space.

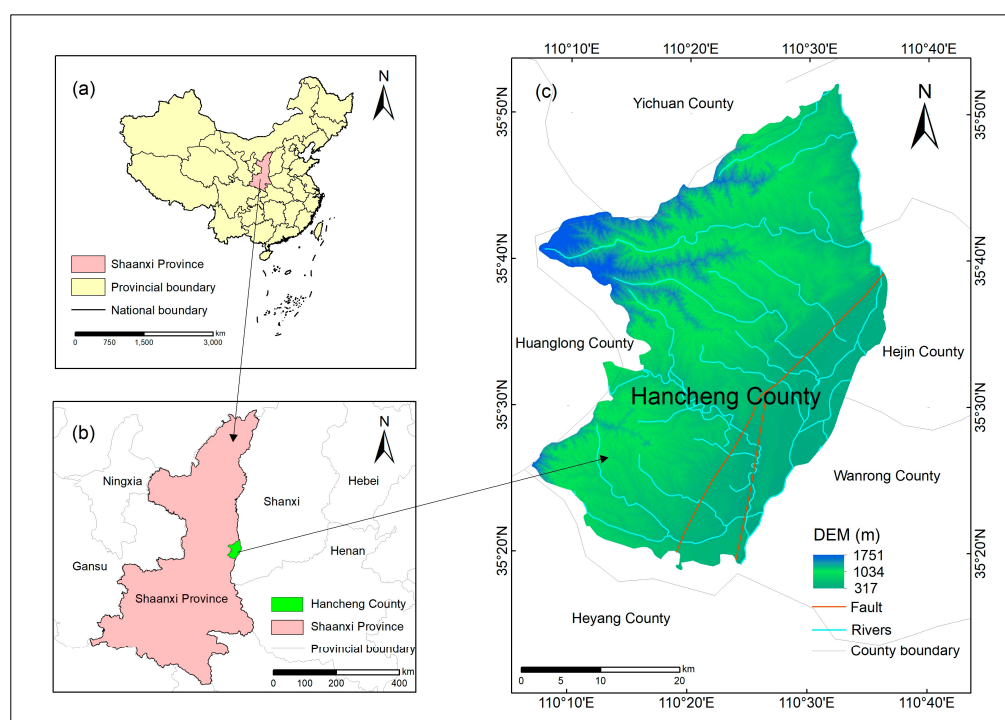


Figure 1. Location map of Hancheng County.

3. Data and Method

3.1. Data

The remote sensing images in this study were mainly obtained from the Google Earth platform. Google Earth is a geographic information software developed by Google, which provides satellite images, map data, 3D models of the Earth, and other functions, allowing users to explore all corners of the Earth virtually. Since its launch in June 2005, Google Earth has attracted a lot of attention from scholars due to its user interface and rich underlying graphics. In November 2016, Google Earth Timelapse was updated to allow users to see the changes in the land surface between 1984 and 2016 (32 years) through the Google Earth platform [26]. Today, the Google Earth platform can provide remote sensing imagery of the present time. The abundant satellite image sources and remote sensing images provided by the Google Earth platform over different periods have offered great convenience for landslide interpretation work [27,28]. Figure 2 shows satellite imagery from three different

historical periods. The comparison of satellite images from different periods can lead to more accurate identification of landslide traces.



Figure 2. Google Earth images in three different years: (a) 2018, (b) 2020, (c) 2022.

3.2. Method

The main methods of landslide interpretation include field surveys, human-computer interactive visual interpretation, automatic extraction, etc. [29].

A field survey is a survey in which researchers observe the morphological characteristics of the landslide at close range, and delineate the approximate range on the geological map. Since field surveys often require a lot of time and labor, especially in complex terrain or large areas, they have limited feasibility in the identification of landslides in large-scale areas as it is difficult to meet the real-time requirements. Thus, this method is only suitable for small-scale areas. Human-computer interactive visual interpretation and automatic extraction methods are currently the two mainstream methods for landslide interpretation [30,31]. Although the automatic extraction method exhibits high efficiency, some problems need to be improved on. For example, several factors may affect the accuracy of the results, including high vegetation coverage, areas with light and shadow, different types of remote sensing images, and different seasons [32,33]. This method is more suitable for the rapid assessment of sudden landslide hazards.

Hancheng is located in the Loess Plateau, where the geological conditions are fragile and complex. Furthermore, it is located at the junction of the tectonically active area. Given this context, there are many landslides in the area, and thus the field survey method is not suitable for this study. Although landslides can be automatically identified at present, the development of this methodology is not fully mature. Automatic identification technology cannot accurately identify long-distance landslides or compound landslides with large-scale development or complex formation mechanisms, so it cannot meet our requirements. Thus, the method selected for this study is human-computer interactive visual interpretation. Based on my previous research experience and my long-term work practice in landslide traces, this study lists a set of objective and effective landslide trace interpretation standards to ensure the authenticity and accuracy of landslide data. In the visual interpretation of human-computer interaction, observing the shape characteristics of landslides is a key step [34]. Landslides often have a typical arch or curved shape, and the edges may be irregular, exhibiting smooth or granular characteristics [35]. Changes in terrain are an important basis for visual interpretation. Features such as surface depressions, cracks, and sliding folds may be signs of a landslide. Differences in color between the landslide area and the surrounding area are also a key point for visual interpretation. Newly formed landslides may show a different color from the surrounding features, such as the color of exposed soil, rocks, or weeds [36,37]. The three-dimensional features of Google Earth images can be used to magnify the morphological appearance of the terrain in order to reveal subtle morphological changes, and the longitude and latitude grids provided by the platform can be added for grid-by-grid landslide interpretation. By adding vector polygons

to circle the boundaries of the landslide, the zoom in and out tools can be used to adjust in situations where the full picture of the landslide cannot be recognized.

Table 1 shows typical landslide identification standards. Based on the above criteria, high-resolution satellite remote sensing interpretation technology was used to carry out the interpretation of landslides in Hancheng County, Shaanxi Province, China, and then a database of landslide traces in Hancheng County was established. The establishment of this landslide database in Hancheng provides the most important data basis for subsequent research on landslides in Hancheng County, providing context for the analysis of the spatial distribution of landslides, the assessment of regional landslide susceptibility, and landslide risk assessment.

Table 1. Typical signs of landslide identification.

Landslide Identification Signs	Description
morphology	The distribution of the landslide body is irregular and staircase-like, and there are cracks in it, mainly located in the middle and the leading edge, which are important markers of landslide activity.
color	Newly formed landslides may show a different color from surrounding features, such as the color of exposed soil, rocks, or weeds.
vegetation	The vegetation texture is discontinuous, and the vegetation on the landslide body presents the pattern of saber trees and drunken forests.

4. Results and Analysis

4.1. Typical Landslide Display

Four typical landslides identified in the study area were selected for display. In the landslide shown in Figure 3a, the posterior wall of the landslide is missing, and the landslide body is piled up at the bottom of the landslide along the sliding direction. From Figure 3b, it can be seen that there is a certain sense of boundary between the landslide and the surrounding terrain environment. From Figure 3c, we can see that the landslide body is piled up on the back wall of the landslide, and in the landslide shown in Figure 3d, it can be seen that the landslide body caused certain scratches to the terrain in the process of sliding. From the four typical landslides shown, it can be seen that the landslide scale in the study area is relatively small. In the process of identifying landslides, we can not only understand the morphology and development scale of individual landslides, but also provide a reliable basis for future research on the distribution law of landslides and associated risk assessment.

4.2. Landslide Database

Based on the high-resolution remote sensing images provided by the Google Earth platform, we identified a total of 6785 landslides in the study area using visual interpretation, and the landslide distribution map is shown in Figure 4. It can be seen from Figure 4 that the landslide traces in Hancheng County are densely distributed on the whole, and there are relatively few landslide traces in the western area. The landslides are mainly distributed in the central area of Hancheng County. In the area near the Yellow River Basin in the east, the landslides are distributed linearly. Figure 5 shows the density distribution of landslide sites in Hancheng County. As can be seen from Figure 5, the landslide distribution density is up to 29.93 km^{-2} , which is due to the abnormal development of landslides in this area. This abnormal development is due to the fact that the Hancheng fault passes through the central part of Hancheng County, causing surface rupture in the central part of the region. The high-density nature of this landslide area is very rare not only in Shaanxi Province, but across the whole country. The above findings provide key clues for further studies on landslide disaster risk in the region.

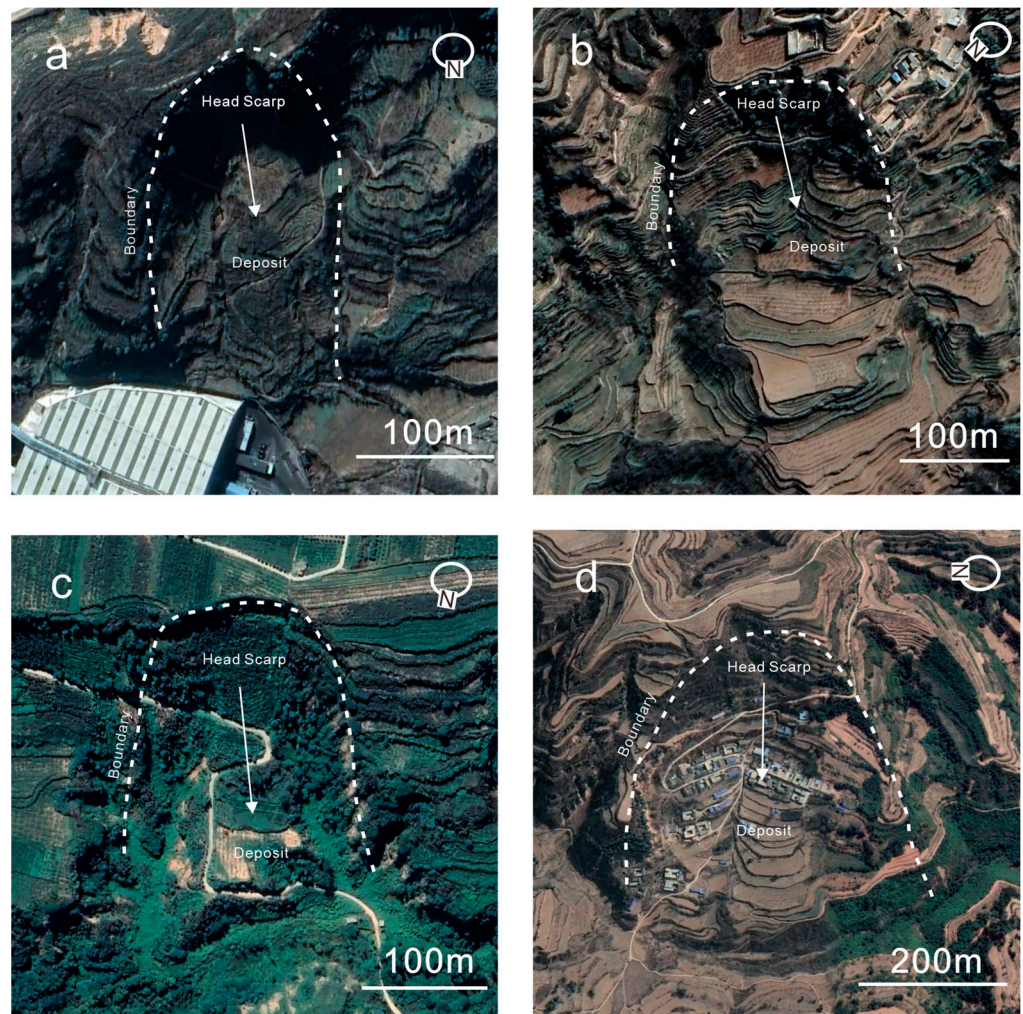


Figure 3. Typical landslides in the study area.

According to the statistics of the single landslide area in Hancheng, the cumulative landslide area is 95.38 km², the average area is 1406.04 m², the maximum landslide area is 377,841 m², and the minimum landslide area is 202.96 m². Among them, there are 248 landslides less than 10³ square meters, 3631 landslides of 10³–10⁴ square meters, 2839 landslides of 10⁴–10⁵ square meters, and only 67 landslides of more than 10⁵ square meters, accounting for 3.66%, 53.52%, 41.84%, and 0.98% of the total landslides, respectively. The cumulative frequency curve shows the trend of the relative frequency of the landslide area value from 0 to 100% (Figure 6). From the curve, it can be seen that the landslide area between 10³ and 10⁴ is the most prominent, which is consistent with the statistical results of the numerical values.

4.3. Landslide Analysis

According to the scale of the landslides, the overall characteristics of landslide development in the area are of a small to medium-scale. From Figure 4, it can be seen that the landslide near the Hancheng fault is relatively developed, which may be related to the fragmentation of the rock strata near the fault. Landslides form easily in this area; both sides of the tributaries of the river are also main development sites for landslide disasters in the study area. There are many river systems in this area, the land is fertile, human habitation is dense, the Quaternary alluvial formation of sand and loess is widely distributed, and the soil is loose, and made looser due to frequent human activities. According to the landslide density distribution map in Figure 5, the distribution of landslide traces in Hancheng has obvious regional characteristics, and the landslides are mainly distributed in the central

area of Hancheng. The distribution of landslides also shows obvious aggregation (Figure 7). Figure 7 shows a landslide cluster at 110.460° E and 35.780° N. The landslides in this area are very concentrated, and the evolution law of landslides is relatively complex, so it is necessary to focus on further scientific research in this landslide concentration area in future.

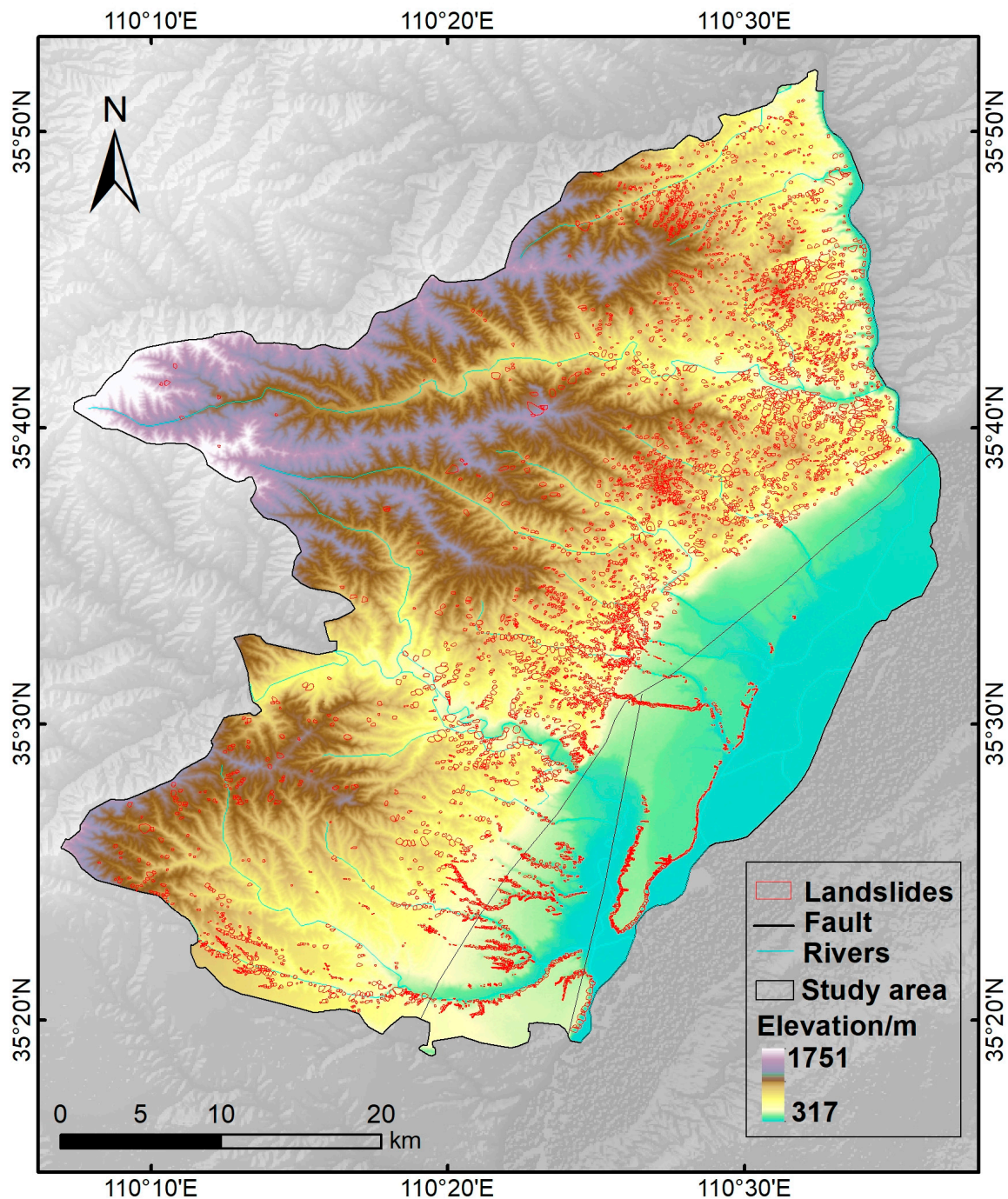


Figure 4. Landslide inventory map of Hancheng County.

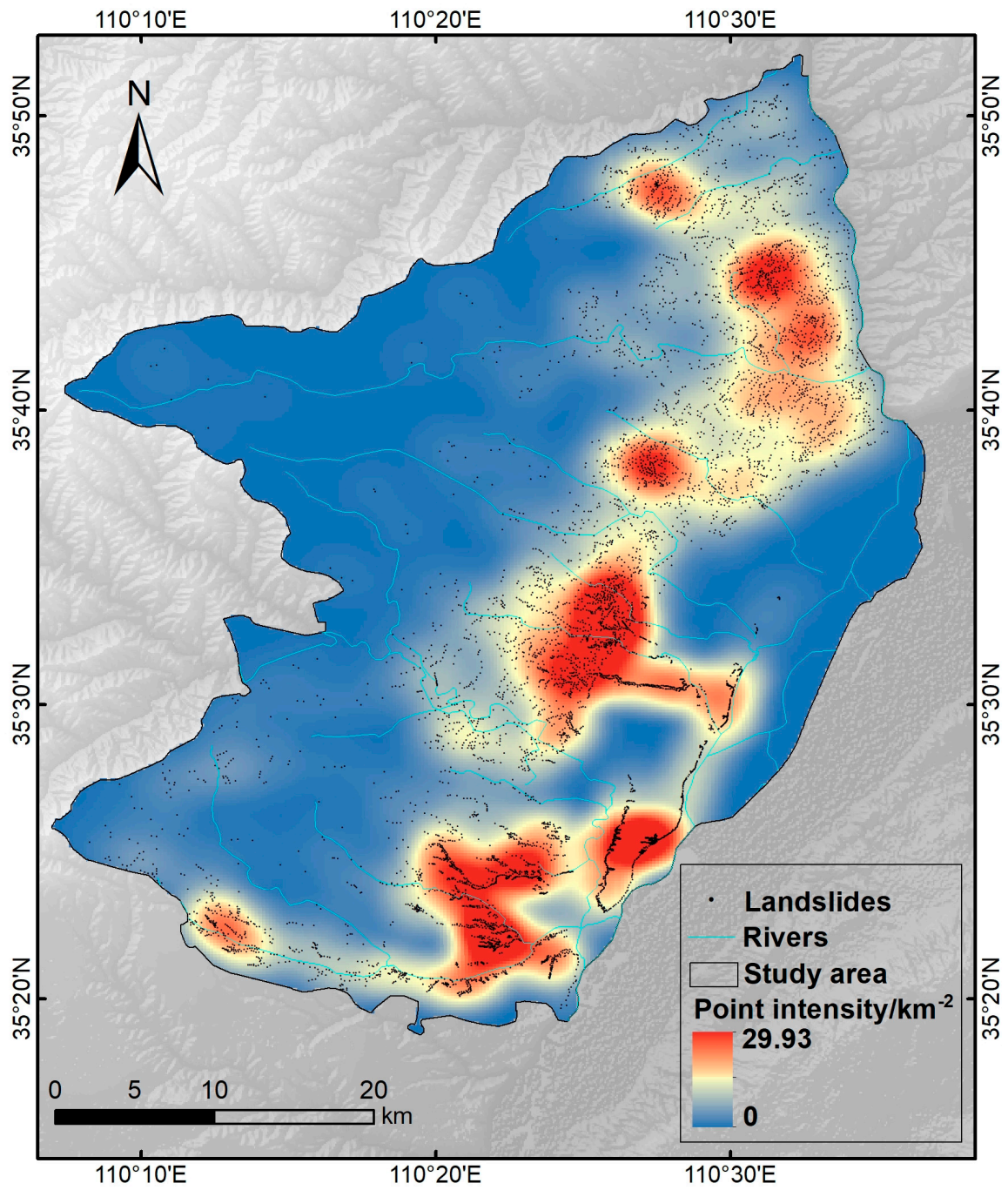


Figure 5. Density distribution of landslide points in Hancheng County.

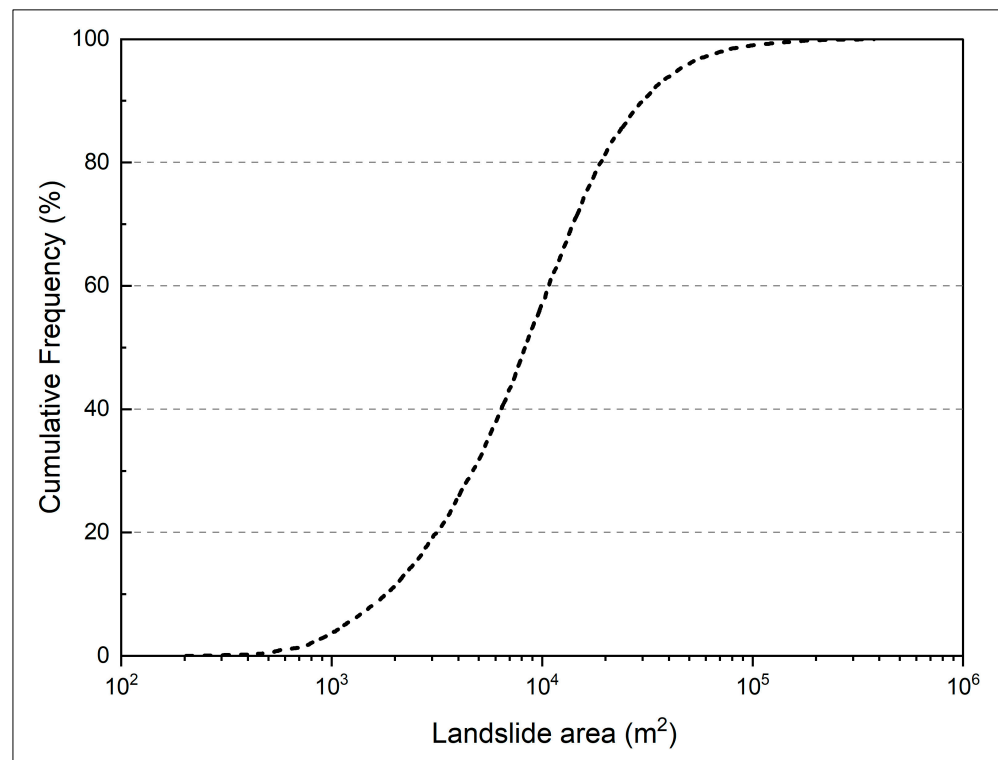


Figure 6. Density distribution of landslide points in Hancheng County.



Figure 7. Landslide cluster map in the study area. (the yellow arrows in the figure indicate the direction of the landslide).

Overall, there are a large number of landslide remnants in Hancheng County. Among them, the distribution is most concentrated in the central and eastern parts, mainly within 3 km to the west of the Hancheng fault. These detailed landslide distribution data provide important basic information for geological disaster risk assessment and geological disaster prevention and control work in the area in the future.

5. Discussion

Significant progress has been made in the research of landslides worldwide, including in the automatic identification of landslides [38,39], landslide susceptibility and risk assessment [40–42], and the mechanism analysis of individual landslides [43,44]. However, there is still a relative lack of work on the establishment of landslide data inventories in all parts of the world. The establishment of a landslide database is the basis for landslide-related research, and a detailed landslide database in a region can provide effective support for the prevention and control of local landslide disasters. Globally, landslides occur with a wide geographical distribution and different frequencies [45–49]. From the tropics to the cold zone, from the mountains to the plains, landslides are possible. However, due to differences in geological, climatic, and ecological characteristics, there are great differences in the frequency and scale of landslides in different regions. For example, the United States is a mountainous country, especially in the western region. Landslides mainly occur during the rainfall season, especially in spring and winter [50–52]. In addition, seismic activity is also an important factor in triggering landslides [53–55]. Japan is an island nation located in the Pacific Rim seismic zone, and earthquakes and rainfall are very frequent. Landslide disasters in Japan are also affected by its unique mountainous and hilly terrain [56,57]. Many parts of Italy are also threatened by landslides [58,59]. In regions such as the Alps and the Apennines, rainfall and snowmelt are the main factors contributing to landslides [60–62]. The Chinese city of Hancheng is located on the Loess Plateau. The Loess Plateau is located in China's geological tectonic ecotone, with faults and folds, and other geological structures, which leads to complex geological structures and fragmented surfaces [63]. In addition, many rivers pass through the territory of Hancheng, resulting in serious soil erosion problems, which in turn leads to frequent landslides. Secondly, climatic factors also have an important effect on the development of landslides in Hancheng County. Rainfall in Hancheng County is mainly concentrated in July and August in summer, and the rainfall intensity is relatively high, which is more likely to increase the risk of landslides. Therefore, it is of great significance to study the landslide database of Hancheng County.

5.1. Comparison with Landslide Databases in Other Parts of the Loess Plateau in China

The creation of a landslide database can help to understand the distribution of landslides more clearly and promote the development of landslide evaluation. In recent years, some scholars have studied the lists of landslides located in other areas on the Loess Plateau, as shown in Table 2. Xu et al. used high-resolution satellite imagery to investigate about 80,000 landslides on the Loess Plateau [64]. Li et al. used multi-temporal high-resolution remote sensing images provided by the Google Earth platform to perform manual visual interpretation of all large-scale landslides (area > 5000 m²) in Baoji City, China [65]. A total of 3422 landslides were identified, with a total landslide area of 360.7 km². Chen et al. used high-resolution optical satellite imagery from the Google Earth platform to map a large-scale landslide in Xianyang, Shaanxi Province, China [66]. Once mapped, a comprehensive and detailed list of 2924 large landslides was obtained. Subsequently, the spatial distribution of the landslide was analyzed based on seven influencing factors, including elevation, slope angle, aspect, curvature, lithology, distance from the river, and distance from the fault. Huang et al. carried out a detailed interpretation of paleo landslides in the middle section of the northern foothills of the Qinling Mountains south of Xi'an, China [67], and interpreted 43 paleo landslides, mainly distributed in the range of 70 km × 10 km, with a total landslide area of 16.57 km². Zhang et al. established a landslide database in Luliang by conducting a large-scale landslide inventory in Luliang City in the eastern part of the Loess Plateau. The landslide mobility level (H/L) of 12,110 landslides in the study area was analyzed, and it was found that there was a linear relationship between landslide height and sliding distance [68].

Table 2. List of landslides in different areas of the Loess Plateau.

No.	Location	Landslide Number	Landslide Area (km ²)	Area of the Study Area (km ²)	Landslide Point Density (km ⁻²)	Source
1	Loess Plateau	80,000	\	300,000	0.27	[64]
2	Baoji City, Shaanxi Province, China	3422	360.7	18,100	0.19	[65]
3	Xianyang City, Shaanxi Province, China	2924	228.66	10,196	0.29	[66]
4	The northern foothills of the Qinling Mountains in China	43	16.57	700	0.06	[67]
5	Luliang City, Shanxi Province, China	12,110	\	21,000	0.58	[68]

In this study, we used optical remote sensing images and human-computer interaction visual interpretation methods to investigate landslides in Hancheng County, China and created a corresponding landslide database. The density of landslide points is the ratio of the total number of landslides in the study area to the area of the study area, and the landslide point density values in the above five areas have been listed in the table. The density of landslide points in Hancheng is 4.19, which shows that landslides in Hancheng have a high incidence, and more in-depth research on landslide disasters in Hancheng is needed to reduce the losses of life and property associated with these disasters.

5.2. Advantages and Limitations of Study Methods

In this study, the human-computer interactive visual interpretation method is used to analyze and delineate landslide boundaries based on visual observation of the color, texture, morphology, and other characteristics of the landslide on the remote sensing image by the interpreter, and combined with other auxiliary data. From the perspective of research methods, optical remote sensing can work around the clock and is not limited by cloud interference. In areas with a lot of clouds, optical remote sensing can penetrate the clouds and obtain high-resolution images of the surface. The human-computer interaction visual interpretation method can make full use of human visual perception and cognitive ability to subjectively interpret and analyze remote sensing images. This helps to extract more useful landslide information from remote sensing imagery. Second, human-computer interaction visual interpretation can reduce the possibility of human error. By working together and combining both elements for validation, the impact of personal biases and misunderstandings on the results can be reduced. However, there are some limitations to this method. This method still depends on the experience and knowledge levels of the interpreter, and cannot deliver high efficiency in the face of sudden landslide disasters and large-scale geological disasters.

5.3. Future Outlook

- (1) We did not explore the reasons for the concentrated distribution of landslides (as shown in Figure 6). In the future, we can study these landslide clusters to better understand the formation and evolution of landslides in Hancheng County.
- (2) In this study, we did not classify the landslide types in detail, and we used the term “landslide traces” to cover all types of mass movement, including landslides, flows, debris flows, etc. [69]. The landslides we interpreted were only landslides with signs of sliding, including all landslide types such as rainfall landslides and earthquake landslides, and the landslides can be classified based on this research result.
- (3) At present, the landslide traces established in this study only include the boundary information of landslides, and we will superimpose the topographic and geological

information (such as slope, aspect, etc.) of Hancheng County into each landslide attribute to analyze the spatial distribution of landslides in the region.

- (4) In this study, only landslides that occurred in Hancheng County were studied, and other types of disasters were not studied. Therefore, in the future, disaster analysis in the Hancheng area should further carry out risk assessment for various disasters (collapse, landslide, debris flow, etc.), fully study and improve understanding of the characteristics of geological disasters in the Hancheng area, and lay the foundation for disaster prevention and mitigation in the area.

6. Conclusions

Based on the high-resolution remote sensing satellite images obtained by the Google Earth platform, this paper carried out human-computer interactive visual interpretation of the 1621 km² area of Hancheng County, Shaanxi Province. A landslide distribution map containing 6785 landslides was drawn. Among them, the total area of recorded landslides was about 95.38 km², accounting for 5.88% of the total area of the study area, the average landslide area was 1406.04 m², the largest landslide area was 377,841 m², and the smallest landslide area was 202.96 m². According to the number and density of landslides, the distribution of landslide development in the study area was analyzed. The results showed that these landslide remnants were mainly concentrated in the middle of the study area, mainly within 3 km west of the Hancheng fault. Compared with previous studies, this study obtained the most complete landslide database yet for Hancheng. The human-computer interaction visual interpretation method used in this study was selected for its capability to more accurately identify some subtle features by combining the professional experience and judgment of an interpreter with the power of technology in order to improve the accuracy of landslide identification. The landslide database obtained in this study can provide an important basis for the formulation of landslide disaster prevention strategies and emergency management measures in the region. On this basis, the causal mechanisms and evolution model for landslides in Hancheng County were further studied, and the accuracy of subsequent landslide susceptibility assessments and risk assessments was improved, providing scientific support for the sustainable development of the region.

Author Contributions: C.X. and X.H. proposed the research concept and provided basic data; C.X. provided basic data; J.Z. processed the initial data and wrote the manuscript. All authors have read and agreed to the published version of the manuscript.

Funding: This research was funded by the National Key Research and Development Program of China (2021YFB3901205) and the National Institute of Natural Hazards, Ministry of Emergency Management of China (2023-JBKY-57).

Institutional Review Board Statement: Not applicable.

Informed Consent Statement: Not applicable.

Data Availability Statement: All data is included in the article.

Acknowledgments: We are grateful to the anonymous reviewers for their constructive comments and suggestions that improved the quality of the manuscript.

Conflicts of Interest: The authors declare no conflicts of interest.

References

1. Xu, X.; Xu, C. Natural Hazards Research: An eternal subject of human survival and development. *Nat. Hazards Res.* **2021**, *1*, 1–3. [[CrossRef](#)]
2. Huang, R. Large-scale landslides in China since the 20th century and their occurrence mechanisms. *Chin. J. Rock Mech. Eng.* **2007**, *26*, 433–454.
3. Highland, L.M.; Bobrowsky, P. *The Landslide Handbook—A Guide to Understanding Landslides*; US Geological Survey: Reston, Virginia, 2008.
4. Cheng, Y. Current status and dynamics of landslide research in China in the past 20 years. *Geol. Hazard Environ. Prot.* **2003**, *14*, 1–5.

5. Wang, X.; Wang, Y.; Lin, Q.; Li, N.; Zhang, X.; Zhou, X. Population risk assessment of landslide disasters in China under climate change. *Clim. Chang. Res.* **2022**, *18*, 166.
6. Wang, T.; Liu, J.; Li, Z.; Xin, P.; Shi, J.; Wu, S. Risk Assessment of Earthquake Landslides in China and Its Impact on Territorial Spatial Planning. *Geol. China* **2021**, *48*, 21–39.
7. Lv, Z.; Yang, T.; Lei, T.; Zhou, W.; Zhang, Z.; You, Z. Spatial-Spectral Similarity based on Adaptive Region for Landslide Inventory Mapping with Remote Sensed Images. In *IEEE Transactions on Geoscience and Remote Sensing*; IEEE: Piscataway, NJ, USA, 2024.
8. Zhang, X.; Jing, Y.; Wang, Y.; Qi, Z.; Wang, Y. Evaluation of landslide susceptibility based on multi-objective optimization method. *J. Soil Water Conserv.* **2024**, *38*, 104–112.
9. Shan, X.; Ye, H.; Li, Z.; Chen, G. remote sensing, GIS combination and regional natural landslide investigation. *Geol. Rev.* **2001**, *47*, 648–652.
10. Mandal, B.; Mondal, S.; Mandal, S. Modelling and mapping landslide susceptibility of Darjeeling Himalaya using geospatial technology. In *Applied Geomorphology and Contemporary Issues*; Springer: Berlin/Heidelberg, Germany, 2022; pp. 565–585.
11. Harp, E.L.; Keefer, D.K.; Sato, H.P.; Yagi, H. Landslide inventories: The essential part of seismic landslide hazard analyses. *Eng. Geol.* **2011**, *122*, 9–21. [[CrossRef](#)]
12. Pennington, C.; Freeborough, K.; Dashwood, C.; Dijkstra, T.; Lawrie, K. The National Landslide Database of Great Britain: Acquisition, communication and the role of social media. *Geomorphology* **2015**, *249*, 44–51. [[CrossRef](#)]
13. Taylor, F.E.; Malamud, B.D.; Freeborough, K.; Demeritt, D. Enriching Great Britain's National Landslide Database by searching newspaper archives. *Geomorphology* **2015**, *249*, 52–68. [[CrossRef](#)]
14. Rabby, Y.W.; Li, Y. Landslide inventory (2001–2017) of Chittagong hilly areas, Bangladesh. *Data* **2019**, *5*, 4. [[CrossRef](#)]
15. Bejenaru, A.; Niculiță, M. Landslide inventory of the Crasna catchment, Moldavian Plateau, Romania. In Proceedings of the Romanian Geomorphology Symposium, Iasi, Romania, 11–14 May 2017.
16. Fusco, F.; Tufano, R.; De Vita, P.; Di Martire, D.; Di Napoli, M.; Guerriero, L.; Mileti, F.A.; Terribile, F.; Calcaterra, D. A revised landslide inventory of the Campania region (Italy). *Sci. Data* **2023**, *10*, 355. [[CrossRef](#)] [[PubMed](#)]
17. Xu, C.; Xu, X.; Shyu JB, H.; Gao, M.; Tan, X.; Ran, Y.; Zheng, W. Landslides triggered by the 20 April 2013 Lushan, China, Mw 6.6 earthquake from field investigations and preliminary analyses. *Landslides* **2015**, *12*, 365–385. [[CrossRef](#)]
18. Pan, J. Identification and distribution of paleolandslides in the eastern section of the Jiangnan Orogenic Belt. *Fujian Build. Mater.* **2022**, *3*, 30–32+36.
19. Huang, Y.; Xie, C.; Li, T.; Xu, C.; He, X.; Shao, X.; Xu, X.; Zhan, T.; Chen, Z. An open-accessed inventory of landslides triggered by the MS 6.8 Luding earthquake, China on 5 September 2022. *Earthq. Res. Adv.* **2023**, *3*, 100181. [[CrossRef](#)]
20. Hong, J.; Wu, S.; Mu, X. Establishment of landslide database and geological characteristics of landslide regional distribution in Gansu Province. *J. Gansu Acad. Sci.* **1991**, *3*, 54–60.
21. Lin, B.; Zhao, F.; Xie, X.; Song, F. Spatial distribution characteristics and causes of urban geological disasters in Hancheng County. *J. Eng. Geol.* **2004**, *12*, 162–165.
22. Cui, Z.; Li, S.; Yang, Z. Deformation Mechanism and Stability Analysis of Slope of Hancheng Power Plant. *J. Catastrophology* **1994**, *9*, 50–54.
23. He, X.; Wang, Z.; Zhong, J.; Liu, X. Deep monitoring and deformation analysis of landslide in Hancheng Power Plant. *J. Nat. Disasters* **2014**, *3*, 119–124.
24. Zhang, X.; Tao, F. Analysis of the Genesis Mechanism and Stability of Loess Landslide in Weibei Plateau Area: A Case Study of Loess Landslide in Chengbei Village, Hancheng County. *Geol. Hazard Environ. Prot.* **2015**, *2*, 3–8.
25. Lin, B.; Zhao, F.; Shi, B. Spatial distribution and prevention of geological disasters in Hancheng City, Shaanxi Province. *J. Catastrophology* **2004**, *19*, 35–39.
26. Jiang, S.; Zhou, L.; Ma, H.; Zhu, W.; Ni, J.; Ma, S.; Zhang, J.; Xun, H. Analysis of Coastline Change in Dalian City Based on Historical Google Earth Imagery. *Geol. Resour.* **2024**, *33*, 56–64.
27. Zeng, T.; Wang, L.; Zhang, Y.; Cheng, P.; Wu, F. Modeling and Interpretability of Landslide Susceptibility Based on CatBoost-SHAP Model. *Chin. J. Geol. Hazard Control.* **2024**, *35*, 37–50.
28. Harvey, E.; Rosser, N.; Kincey, M.; Densmore, A.; Shrestha, R.; Pujara, D.; Dunant, A.; de Vries Max Van Wyk Arrell, K. Using Google Earth Engine to map landslide hazard and exposure across Nepal. In Proceedings of the Copernicus Meetings, Vienna, Austria, 14–19 April 2024. EGU24-15272.
29. Wang, Y.; Ren, G.; Wang, J.; Wang, M.; Yu, T. A review of remote sensing interpretation of landslides. *Northwest Hydropower* **2017**, *1*, 17–21.
30. Fiorucci, F.; Ardizzone, F.; Mondini, A.C.; Viero, A.; Guzzetti, F. Visual interpretation of stereoscopic NDVI satellite images to map rainfall-induced landslides. *Landslides* **2019**, *16*, 165–174. [[CrossRef](#)]
31. Liu, P.; Wei, Y.; Wang, Q.; Xie, J.; Chen, Y.; Li, Z.; Zhou, H. A research on landslides automatic extraction model based on the improved mask R-CNN. *ISPRS Int. J. Geo-Inf.* **2021**, *10*, 168. [[CrossRef](#)]
32. Dai, F.C.; Xu, C.; Yao, X.; Xu, L.; Tu, X.B.; Gong, Q.M. Spatial distribution of landslides triggered by the 2008 Ms 8.0 Wenchuan earthquake, China. *J. Asian Earth Sci.* **2011**, *40*, 883–895. [[CrossRef](#)]
33. Huang, F.; Tao, S.; Chang, Z.; Huang, J.; Fan, X.; Jiang, S.-H.; Li, W. Efficient and automatic extraction of slope units based on multi-scale segmentation method for landslide assessments. *Landslides* **2021**, *18*, 3715–3731. [[CrossRef](#)]

34. Cai, J.; Ming, D.; Zhao, W.; Lin, X.; Zhang, Y.; Zhang, X. Identification of Landslide Hazards and Disaster Mechanism Analysis in Chayu County Based on Integrated Remote Sensing. *Remote Sens. Nat. Resour.* **2024**, *36*, 128–136.
35. Dias, H.C.; Grohmann, C.H. Standards for shallow landslide identification in Brazil: Spatial trends and inventory mapping. *J. South Am. Earth Sci.* **2024**, *135*, 104805. [[CrossRef](#)]
36. Lillesand, T.; Kiefer, R.W.; Chipman, J. *Remote Sensing and Image Interpretation*; John Wiley & Sons: Hoboken, NJ, USA, 2015.
37. Shao, X.; Xu, C.; Li, L.; Yang, Z.; Yao, X.; Shao, B.; Liang, C.; Xue, Z.; Xu, X. Spatial analysis and hazard assessment of Large-scale ancient landslides around the reservoir area of Wudongde Hydropower Station, China. *Nat. Hazards* **2024**, *120*, 87–105. [[CrossRef](#)]
38. Yu, B.; Xu, C.; Chen, F.; Wang, N.; Wang, L. HADeenNet: A hierarchical-attention multi-scale deconvolution network for landslide detection. *Int. J. Appl. Earth Obs. Geoinf.* **2022**, *111*, 102853. [[CrossRef](#)]
39. Sreelakshmi, S.; Chandra, S.S.V. Visual saliency-based landslide identification using super-resolution remote sensing data. *Results Eng.* **2023**, *21*, 101656. [[CrossRef](#)]
40. Klimeš, J.; Novotný, J.; Balek, J.; Rosario, A.M.; Torres-Lázaro, J.C.; Vargas, R.; López, D.; Obispo, Y.; Roldán-Minaya, E.; Caballero, A. Landslide hazard assessment and risk reduction in the rural community of Rampac Grande, Cordillera Negra, Peru. *Environ. Earth Sci.* **2024**, *83*, 27. [[CrossRef](#)]
41. Liu, F.; Wang, L.; Xiao, D. Application of Machine Learning Model in Landslide Vulnerability Assessment. *Chin. J. Geol. Hazard Control.* **2021**, *32*, 98–106.
42. Zhang, Z.; Deng, M.; Xu, S.; Zhang, Y.; Fu, H.; Li, Z. Comparative study on landslide susceptibility evaluation model in Zhenkang County. *Chin. J. Rock Mech. Eng.* **2022**, *41*, 157–171.
43. Sajwan, A.; Mhasiki, S.; Pandey, A.; Vangla, P.; Ramana, G.V. A multi-scale approach for deterministic analysis of landslide triggering and mass flow mechanism at Kaliyasaur (Rudraprayag). *Landslides* **2024**, *21*, 393–409. [[CrossRef](#)]
44. Jiang, T.; Cui, S.; Ran, Y. Analysis of landslide mechanism induced by coupling excavation and rainfall. *Chin. J. Geol. Hazard Control.* **2023**, *34*, 20–30.
45. Carrión-Mero, P.; Montalván-Burbano, N.; Morante-Carballo, F.; Quesada-Román, A.; Apolo-Masache, B. Worldwide research trends in landslide science. *Int. J. Environ. Res. Public Health* **2021**, *18*, 9445. [[CrossRef](#)]
46. Wang, Y.; Tang, G.; Fang, Z.; Li, P. Prediction of Disaster Occurrence of Global-scale Landslide Disasters Based on Automated Machine Learning. *Resour. Environ. Eng.* **2022**, *18*, 1–90.
47. Felsberg, A.; Poesen, J.; Bechtold, M.; Vanmaercke De Lannoy, G.J.M. Estimating global landslide susceptibility and its uncertainty through ensemble modelling. *Nat. Hazards Earth Syst. Sci. Discuss.* **2021**, *2021*, 3063–3082.
48. Santangelo, M.; Althuwayne, O.; Alvioli, M.; Ardizzone, F.; Bianchi, C.; Bornaetxea, T.; Brunetti, M.; Bucci, F.; Cardinali, M.; Donnini, M.; et al. Inventory of landslides triggered by an extreme rainfall event in Marche-Umbria, Italy, on 15 September 2022. *Sci. Data* **2023**, *10*, 427. [[CrossRef](#)] [[PubMed](#)]
49. Devoto, S.; Hastewell, L.J.; Prampolini, M.; Furlani, S. Dataset of gravity-induced landforms and sinkholes of the northeast coast of Malta (Central Mediterranean Sea). *Data* **2021**, *6*, 81. [[CrossRef](#)]
50. Mirus, B.B.; Jones, E.S.; Baum, R.L.; Godt, J.W.; Slaughter, S.; Crawford, M.M.; Lancaster, J.; Stanley, T.; Kirschbaum, D.B.; Burns, W.J. Landslides across the USA: Occurrence, susceptibility, and data limitations. *Landslides* **2020**, *17*, 2271–2285. [[CrossRef](#)]
51. Zamaniavijeh, N.; Hosseinzadehsabeti, E.; Ferré, E.C.; Hacker, D.B.; Biedermann, A.R.; Biek, R.F. Kinematics of frictional melts at the base of the world's largest terrestrial landslide: Markagunt gravity slide, southwest Utah, United States. *J. Struct. Geol.* **2021**, *153*, 104448. [[CrossRef](#)]
52. Fleming, R.W.; Taylor, F.A. *Estimating the costs of landslide damage in the United States*; US Department of the Interior, Geological Survey: Reston, VA, USA, 1980.
53. Basharat, M.; Riaz, M.T.; Jan, M.Q.; Xu, C.; Riaz, S. A review of landslides related to the 2005 Kashmir Earthquake: Implication and future challenges. *Nat. Hazards* **2021**, *108*, 1–30. [[CrossRef](#)]
54. Cheaib, A.; Lacroix, P.; Zerathe, S.; Jongmans, D.; Ajorlou, N.; Doin, M.-P.; Hollingsworth, J.; Abdallah, C. Landslides induced by the 2017 Mw7.3 Sarpol Zahab earthquake (Iran). *Landslides* **2022**, *19*, 603–619. [[CrossRef](#)]
55. Qiu, H.; Su, L.; Tang, B.; Yang, D.; Ullah, M.; Zhu, Y.; Kamp, U. The effect of location and geometric properties of landslides caused by rainstorms and earthquakes. *Earth Surf. Process. Landf.* **2024**; *Early View*.
56. Ling, S.; Chigira, M. Characteristics and triggers of earthquake-induced landslides of pyroclastic fall deposits: An example from Hachinohe during the 1968 M7.9 Tokachi-Oki earthquake, Japan. *Eng. Geol.* **2020**, *264*, 105301. [[CrossRef](#)]
57. Ito, Y.; Yamazaki, S.; Kurahashi, T. Geological features of landslides caused by the 2018 Hokkaido Eastern Iwate Earthquake in Japan. *Geol. Soc.* **2021**, *501*, 171–183. [[CrossRef](#)]
58. Perrone, A.; Canora, F.; Calamita, G.; Bellanova, J.; Serlenga, V.; Panebianco, S.; Tragni, N.; Piscitelli, S.; Vignola, L.; Doglioni, A. A multidisciplinary approach for landslide residual risk assessment: The Pomarico landslide (Basilicata Region, Southern Italy) case study. *Landslides* **2021**, *18*, 353–365. [[CrossRef](#)]
59. D'Ippolito, A.; Lupiano, V.; Rago, V.; Terranova, O.G.; Iovine, G. Triggering of rain-induced landslides, with applications in southern Italy. *Water* **2023**, *15*, 277. [[CrossRef](#)]
60. Chiarelli, D.D.; Galizzi, M.; Bocchiola, D.; Rosso, R.; Rulli, M.C. Modeling snowmelt influence on shallow landslides in Tartano valley, Italian Alps. *Sci. Total Environ.* **2023**, *856*, 158772. [[CrossRef](#)] [[PubMed](#)]
61. Pigazzi, E.; Bersezio, R.; Marotta, F.; Apuani, T. Mapping landscape evolution in 3D: Climate change, natural hazard and human settlements across the 1618 Piuro landslide in the Italian Central Alps. *Earth Surf. Process. Landf.* **2024**, *49*, 837–854. [[CrossRef](#)]

62. Leonelli, G.; Chelli, A. Spatial distribution patterns of dated landslide events in the Northern Apennines in response to Holocene regional climatic changes. *Catena* **2024**, *236*, 107705. [[CrossRef](#)]
63. Xiong, L.; Tang, G. Research progress and prospect of geomorphological development and evolution of gullies on the Loess Plateau. *J. Geo-Inf. Sci.* **2020**, *22*, 816–826.
64. Xu, Y.; Allen, M.B.; Zhang, W.; Li, W.; He, H. Landslide characteristics in the Loess Plateau, northern China. *Geomorphology* **2020**, *359*, 107150. [[CrossRef](#)]
65. Li, L.; Xu, C.; Xu, X.; Zhang, Z.; Cheng, J. Inventory and Distribution Characteristics of Large-Scale Landslides in Baoji City, Shaanxi Province, China. *ISPRS Int. J. Geo-Inf.* **2022**, *11*, 10. [[CrossRef](#)]
66. Chen, J.; Li, L.; Xu, C.; Huang, Y.; Luo, Z.; Xu, X.; Lyu, Y. Freely accessible inventory and spatial distribution of large-scale landslides in Xianyang City, Shaanxi Province, China. *Earthq. Res. Adv.* **2023**, *3*, 100217. [[CrossRef](#)]
67. Huang, W.; Yang, Q.; Lv, Y.; Su, S.; Zhou, Z. Study on the relationship between the distribution characteristics and seismic activity of paleo landslides in the northern foot of the Qinling Mountains. *J. Geol.* **2020**, *28*, 1259–1271.
68. Zhang, X.; Lei, L.; Xu, C. Large-scale landslide inventory and their mobility in Lvliang City, Shanxi Province, China. *Nat. Hazards Res.* **2022**, *2*, 111–120. [[CrossRef](#)]
69. Hungr, O.; Leroueil, S.; Picarelli, L. The Varnes classification of landslide types, an update. *Landslides* **2014**, *11*, 167–194. [[CrossRef](#)]

Disclaimer/Publisher’s Note: The statements, opinions and data contained in all publications are solely those of the individual author(s) and contributor(s) and not of MDPI and/or the editor(s). MDPI and/or the editor(s) disclaim responsibility for any injury to people or property resulting from any ideas, methods, instructions or products referred to in the content.